ELSEVIER

Chemical Engineering Journal 84 (2001) 397–404

Chemical Engineering Journal

www.elsevier.com/locate/cej

Bubble behavior in gas–liquid–solid three-phase circulating fluidized beds

Tiefeng Wang, Jinfu Wang*, Weiguo Yang, Yong Jin

Department of Chemical Engineering, Tsinghua University, Beijing 100084, PR China

Received 13 September 2000; received in revised form 8 January 2001; accepted 10 January 2001

Abstract

A novel fiber optic probe system has been developed for studying the bubble behavior in gas–liquid–solid three-phase circulating fluidized beds (TPCFBs). Mathematical method to analyze data by probe technique has also been discussed in this paper. The bubble size and its distribution, bubble Sauter diameter, gas–liquid interfacial area and bubble rise velocity, have been experimentally studied using the fiber optic probe. The experimental results show that the bubble size distribution in TPCFBs follows lognormal function. The bubble Sauter diameter has the radial profile with smaller value in the central region than in the near-wall region, different from the conventional three-phase fluidized beds (CTPFBs) without outer particle circulation. The distribution of bubble rise velocity, gas–liquid interfacial area and effect of the operation conditions have been experimentally studied.

Keywords: Three-phase circulating fluidized beds; Bubble size; Bubble velocity; Gas–liquid interfacial area; Fiber optic probe

1. Introduction

Gas–liquid–solid three-phase fluidized beds have been widely used in petrochemical, metallurgical, environmental and coal liquefaction processes [1]. Conventional three-phase fluidized beds without outer particle circulation encounter troubles when applied to systems with catalyst liable to be deactivated or with small/light particles; moreover, the heat removal is a troublesome problem for a strong exothermic reaction. Liang et al. [2] presented a three-phase fluidized bed with outer particle circulation and higher liquid velocity, suitable for light/small particles widely used in biochemical processes. Previous experimental study shows that three-phase circulating fluidized beds (TPCFBs) have better hydrodynamics and mass transfer performance than conventional three-phase fluidized beds (CTPFBs) without outer particle circulation [3–5]. In TPCFBs, the particle circulating rate G_s and solid holdup can be adjusted by regulating the flow ratio between the primary and secondary stream of the liquid, thus, the superficial gas velocity U_g, superficial liquid velocity U_ℓ and particle circulating rate G_s can be independently controlled. This character is of great advantage for reactor design and operation, superior to the three-phase airlift external loop or internal loop reactor with particle and liquid circulation as well.

The bubble behavior, one of the most important parameters for the reactor simulation and design, is related to the phase holdup, interaction of the phases and mass transfer behavior. Remarkable research has been carried out on bubble behavior in CTPFBs [6,7], but no report in TPCFBs was found in the literature. Due to particle circulation and higher liquid velocity, TPCFBs have a special flow structure different from CTPFBs [3]; therefore, the bubble behavior should also has its own special characteristics.

Probe technique is an effective method to measure the bubble properties such as bubble size distribution and bubble rise velocity in three-dimensional three-phase fluidized beds [8]. Several probe methods for measuring bubble properties, such as electrical conductivity probe [6], electrical resistive probe [19], and fiber optic probe [9–11] have been mentioned in literature. The fiber optic probe is applicable both to electric and non-electric system, and the compact structure reduces disturbance to the flow field giving more accurate result. These advantages make the fiber optic fiber preference in recent years.

From the probe signal, we can only get the bubble rise velocity and bubble chord length distribution. The algorithm inferring the bubble size distribution from the measured chord length distribution must be established. Some researchers proposed the algorithm for determining the size distribution of bubbles touching the probe [9,12], however, this bubble size distribution can not be directly used to determine the gas–liquid interfacial area with the given local gas holdup. Liu et al. [8] developed an ana-

* Corresponding author. Tel.: +86-10-62785464; fax: +86-10-62772051.
E-mail address: wangjfu@mail.tsinghua.edu.cn (J. Wang).

1385-8947/01/$ – see front matter
PII: S1385-8947(01)00129-2

Nomenclature

a	gas–liquid interfacial area (m^2/m^3)
d_b	bubble diameter defined with the maximum vertical chord length (mm)
d_{va}	bubble Sauter diameter (mm)
Eo	$g\rho_l d_e^2/\sigma$, the Eötvös number
G_s	Particle circulation rate ($kg\,m^{-2}\,s^{-1}$)
l_b	bubble chord length (mm)
m_b	number of bubbles per unit volume ($1\,m^{-3}$)
Mo	$g\mu_l^4/\rho_l\sigma^3$, the Morton number
P	probability density function ($1\,mm^{-1}$)
r	radial coordinate (mm)
R	radius of the fluidized bed (mm)
R_b	bubble horizontal radius (mm)
u_b	bubble rise velocity (m s)
U_g	superficial gas velocity (m s)
U_ℓ	superficial liquid velocity (m s)

Greek Letters

α	shape factor of the bubble
ε_g	gas phase holdup
ε_s	solid holdup

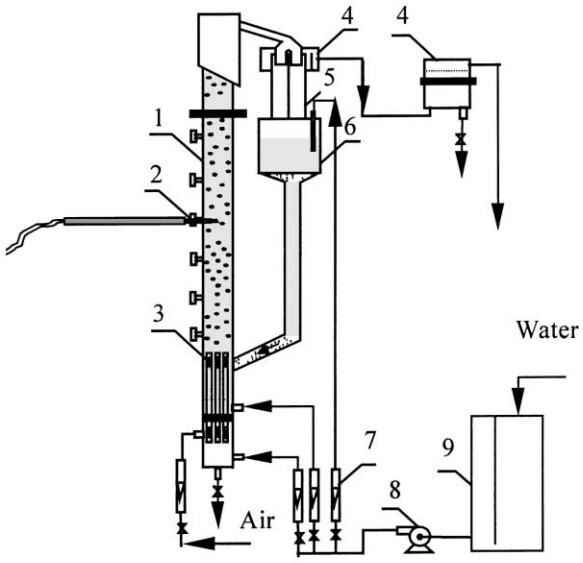

1. Three-phase fluidized bed 2. Fiber optic probe 3. Gas-liquid distributor 4. Liquid-solid separator 5. Particle metering tank 6. Particle reservoir 7. Flowmeter 8. Pump 9. Liquid reservoir.

Fig. 1. Scheme of the experimental apparatus.

lytic and non-parameter backward transform for inferring the size distribution of bubbles through an area element from the chord length dada, but no experimental results using this more accurate algorithm have been found in literature.

In this paper, improvements have been made both to the probe structure and data analysis algorithm. Further discussion such as adjustable threshold method for signal identification, and the relationship between the size distribution of bubbles touching the probe and bubbles in the system as defined in following text, have been made to the Liu's [8] algorithm. Software based on this algorithm has been developed for data processing to give the local gas holdup, bubble size distribution, bubble rise velocity, bubble frequency, and gas–liquid interfacial area.

2. Experimental

A schematic diagram of the experimental apparatus is shown in Fig. 1. The riser is a vertical Plexiglas column 140 mm in inner diameter and 3.0 m in height. Tap water and air are used as the liquid and gas phase, respectively. Glass beads of diameter 0.4 mm and density 2460 kg/m^3 are used as the solid phase. Air is pumped into the bed from the bottom, distributed by a pipe-type gas–liquid distributor and flow up concurrently with the liquid. The liquid pumped from the reservoir is divided into two streams and then fed into the bed. The primary stream fluidizes the particles and the secondary stream control the friction of the particle inlet, thus, the particle circulating rate can be controlled by regulating the flow rate ratio between the two liquid stream. Higher liquid velocity is adopted to ensure the fluidized bed is operated in the three-phase circulating regime [2]. The fiber optic probe connected to the bed-wall is movable in the radial direction so that the bubble behavior in different radial position can be measured.

A novel fiber optic probe system has been developed for measuring the bubble behavior in multiphase flows. Improvements have been made both to the probe structure. The adoption of more tenuous optic fiber with kernel diameter 62.5 μm (in literature, a optic fiber with diameter 1 mm was used, see [9,13]) and technique of emitting and receiving light in the same fiber make the structure more compact, which in turn, diminishes the signal response and the disturbance to the flow field when measuring the bubble parameters. The block diagram of the system is shown in Fig. 2. The emitted light beam is split through the splitter, and then sent into the fiber through the fiber coupler. Each beam is reflected at the end of the fiber. The intensity of the reflected light is different when the probe tip is in the liquid and bubble due to different refraction. The presence of particles in the system has no signal response, this make the developed probe system applicable to both gas–liquid–solid three-phase and gas–liquid two-phase system. The output light density signal containing information of bubble behaviors is transmitted into electrical signal through a light detector, and amplified through the amplifier to output standard voltage signals. The signals are sampled by an analog-to-digital data acquisition-card and the

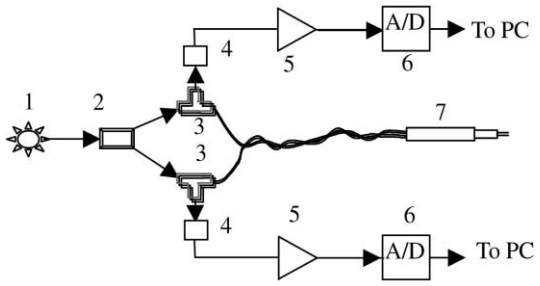

1.Laser source 2. Light splitter 3. Fiber coupler 4. Light detector
5. Amplifier 6. A/D Transducer 7. Probe.

Fig. 2. Hardware structure of the fiber optic probe for bubble measuring.

results are stored into a data file in a PC. A specially written program has been developed to control data acquisition and analysis to the measured data.

3. Algorithm

3.1. Bubble rise velocity

Bubble measurement using fiber optic probe is based on the refraction difference of the gas and liquid. The level of output signal is low when the probe fiber is in the liquid phase, and becomes high when the probe fiber pierces into a gas bubble. When the gas–liquid–solid mixture flows up concurrently, output signal containing bubble information is obtained, as shown in Fig. 3. The downstream signal lags a little compared with the upstream signal due to the distance between the two fibers, which is clearly in the locally enlarge signal Fig. 3. The lag time can be determined by correlation method, and then, with the distance of the fibers, the bubble rise velocity can be calculated [9].

3.2. Bubble chord length distribution

The bubble chord length is calculated by multiplying the bubble rise velocity and the duration time of the probe in the bubble. The bubble signal is not ideally rectangular, therefore, the selection of threshold values has effect on determination of the start and end time of a bubble signal. Single threshold, dual thresholds method and thresholds based on a rate of signal change with time or called slope method have been adopted in the literature, [9,13]. Fixed threshold method may cause the omission of the small bubble or mistake of identifying two adjacent bubble signals as a larger one. The slope method is sensitive to the signal noise and is of poorly robust performance. In this paper, an improved dual threshold method is proposed. In this method, the threshold value varies with the peak value of each bubble signal, which may be smaller for the smaller bubble. The low and high threshold value $V_{\mathrm{lh}i}$ and $V_{\mathrm{hl}i}$ for the ith bubble signal is calculated by

$$V_{\mathrm{lh}i} = V_{\mathrm{l}i} + \gamma(V_{\mathrm{h}i} - V_{\mathrm{l}i}) \quad (1)$$

$$V_{\mathrm{hl}i} = V_{\mathrm{l}i} + (1-\gamma)(V_{\mathrm{h}i} - V_{\mathrm{l}i}) \quad (2)$$

where γ is an adjustable parameter set to be 0.1 in our experiment, $V_{\mathrm{l}i}$ and $V_{\mathrm{h}i}$ the lowest and highest value of the ith bubble signal, respectively. The comparison of the dual adjustable threshold method to single threshold method and dual fixed threshold method is shown in Fig. 4.

3.3. Bubble size distribution

To derive the bubble size distribution from the chord length distribution, the following basic hypothesis are made in advance:

- The bubbles are ellipsoidal with the same shape factor.
- The bubbles are considered to rise in vertical line path.

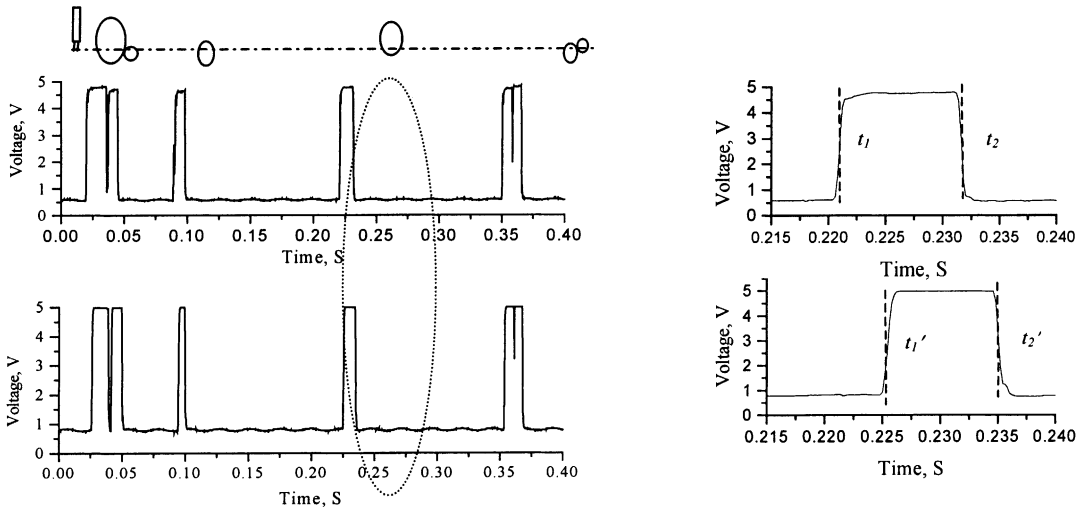

Fig. 3. Typical signals from the optical fiber probe.

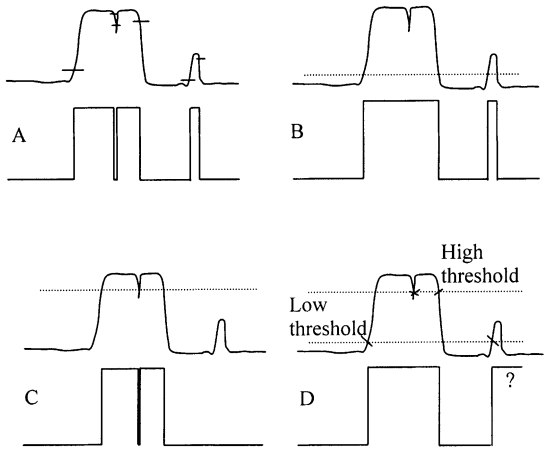

Fig. 4. Comparison between dual adjustable threshold method and other methods in literature.

- The probability of the probe fiber touching a point in the bubble cross-section is the some for every point.

To illuminate the relationship between the bubble chord length distribution and the bubble size distribution, definitions of bubble size distributions are given as follows:

- Size distribution of bubbles touching the probe

$$P_{\mathrm{p}}(d_{\mathrm{b}}) = \lim_{\Delta d_{\mathrm{b}} \to 0} \frac{1}{\Delta d_{\mathrm{b}}} \frac{n_{\mathrm{bp}}(d_{\mathrm{b}}, d_{\mathrm{b}} + \Delta d_{\mathrm{b}})}{n_{\mathrm{bp}}(0, d_{\mathrm{b\,max}})} \tag{3}$$

where $n_{\mathrm{bp}}(d_{\mathrm{b}}, d_{\mathrm{b}} + \Delta d_{\mathrm{b}})$ is the number of bubbles touching the probe with diameter between d_{b} and $d_{\mathrm{b}} + \Delta d_{\mathrm{b}}$, and $n_{\mathrm{bp}}(0, d_{\mathrm{b\,max}})$ the total number of bubbles touching the probe.

- Size distribution of bubbles through a horizontal area element around the probe tip and with $R_{\max}$ as the radius

$$P_{\mathrm{cs}}(d_{\mathrm{b}}) = \lim_{\Delta d_{\mathrm{b}} \to 0} \frac{1}{\Delta d_{\mathrm{b}}} \frac{n_{\mathrm{bcs}}(d_{\mathrm{b}}, d_{\mathrm{b}} + \Delta d_{\mathrm{b}})}{n_{\mathrm{bcs}}(0, d_{\mathrm{b\,max}})} \tag{4}$$

where $n_{\mathrm{bcs}}(d_{\mathrm{b}}, d_{\mathrm{b}}+\Delta d_{\mathrm{b}})$ is the number of bubbles through a horizontal area element with diameter between d_{b} and $d_{\mathrm{b}} + \Delta d_{\mathrm{b}}$, and $n_{\mathrm{bcs}}(0, d_{\mathrm{b\,max}})$ the total number of bubbles through this horizontal area element.

- Size distribution of bubbles in a volume element

$$P_{\mathrm{s}}(d_{\mathrm{b}}) = \lim_{\Delta d_{\mathrm{b}} \to 0} \frac{1}{\Delta d_{\mathrm{b}}} \frac{n_{\mathrm{bs}}(d_{\mathrm{b}}, d_{\mathrm{b}} + \Delta d_{\mathrm{b}})}{n_{\mathrm{bs}}(0, d_{\mathrm{b\,max}})} \tag{5}$$

where $n_{\mathrm{bs}}(d_{\mathrm{b}}, d_{\mathrm{b}} + \Delta d_{\mathrm{b}})$ is the number of bubbles in a volume element with diameter between d_{b} and $d_{\mathrm{b}} + \Delta d_{\mathrm{b}}$, and $n_{\mathrm{bs}}(0, d_{\mathrm{b\,max}})$ the total number of bubbles in this volume element.

Liu et al. [8] have indicated that the relationship between $P_{\mathrm{c}}(l_{\mathrm{b}})$, $P_{\mathrm{p}}(d_{\mathrm{b}})$, and $P_{\mathrm{cs}}(d_{\mathrm{b}})$ as follows:

$$P_{\mathrm{p}}(d_{\mathrm{b}}) = \frac{1}{2}\left[P_{\mathrm{c}}(l_{\mathrm{b}}) - l_{\mathrm{b}}\frac{dP_{\mathrm{c}}(l_{\mathrm{b}})}{dl_{\mathrm{b}}}\right]_{l_{\mathrm{b}}=d_{\mathrm{b}}} \tag{6}$$

$$P_{\mathrm{cs}}(d_{\mathrm{b}}) = \frac{P_{\mathrm{p}}(d_{\mathrm{b}})}{d_{\mathrm{b}}^2}\left[\int_0^\infty \frac{P_{\mathrm{p}}(d_{\mathrm{b}})}{d_{\mathrm{b}}^2}\,\mathrm{d}d_{\mathrm{b}}\right]^{-1} \tag{7}$$

The difference between $P_{\mathrm{c}}(l_{\mathrm{b}})$ and $P_{\mathrm{p}}(d_{\mathrm{b}})$ is due to a bubble touching the probe tip at different position, and the difference between $P_{\mathrm{p}}(d_{\mathrm{b}})$ and $P_{\mathrm{cs}}(d_{\mathrm{b}})$ is due to higher probability of a larger bubble touching the probe tip. Similarly, $P_{\mathrm{s}}(d_{\mathrm{b}})$ is different from $P_{\mathrm{cs}}(d_{\mathrm{b}})$ due to the variation of bubble rise velocity with bubble size, this difference is not considered in Liu's discussion, which is unreasonable especially in system with bubble size varying in a wide range.

$P_{\mathrm{cs}}(d_{\mathrm{b}})$ can be expressed by $P_{\mathrm{s}}(d_{\mathrm{b}})$ in the following way:

$$P_{\mathrm{cs}}(d_{\mathrm{b}}) = \frac{P_{\mathrm{s}}(d_{\mathrm{b}})u_{\mathrm{b}}(d_{\mathrm{b}})}{\int_0^\infty P_{\mathrm{s}}(d_{\mathrm{b}})u_{\mathrm{b}}(d_{\mathrm{b}})\,\mathrm{d}d_{\mathrm{b}}} \tag{8}$$

or

$$\int_0^\infty P_{\mathrm{s}}(d_{\mathrm{b}})u_{\mathrm{b}}(d_{\mathrm{b}})\,\mathrm{d}d_{\mathrm{b}} = \left[\int_0^\infty \frac{P_{\mathrm{cs}}(d_{\mathrm{b}})}{u_{\mathrm{b}}(d_{\mathrm{b}})}\,\mathrm{d}d_{\mathrm{b}}\right]^{-1} \tag{9}$$

Using the unitary property of $P_{\mathrm{s}}(d_{\mathrm{b}})$, derivative with Eq. (9) yields

$$P_{\mathrm{s}}(d_{\mathrm{b}}) = \frac{P_{\mathrm{cs}}(d_{\mathrm{b}})}{u_{\mathrm{b}}(d_{\mathrm{b}})}\left[\int_0^\infty \frac{P_{\mathrm{cs}}(d_{\mathrm{b}})}{u_{\mathrm{b}}(d_{\mathrm{b}})}\,\mathrm{d}d_{\mathrm{b}}\right]^{-1} \tag{10}$$

With Eqs. (6), (7) and (10), the bubble size distribution in the system $P_{\mathrm{s}}(d_{\mathrm{b}})$ can be determined from the measured chord length distribution. Tsuchiya et al. [14] found that the single bubble rising velocity nearly does not vary with bubble size in the range of $2\,\mathrm{mm} < d_{\mathrm{b}} < 10\,\mathrm{mm}$, and experimental result shows that the bubble size in TPCFBs is in this range, therefore, $P_{\mathrm{s}}(d_{\mathrm{b}})$ and $P_{\mathrm{cs}}(d_{\mathrm{b}})$ is considered to be the same in TPCFBs. The difference between $P_{\mathrm{c}}(l_{\mathrm{b}})$, $P_{\mathrm{p}}(d_{\mathrm{b}})$ and $P_{\mathrm{s}}(d_{\mathrm{b}})$ in TPCFBs is shown in Fig. 5.

3.4. Gas–liquid interfacial area

Suppose the number of bubbles per unit volume is m_{b}, the gas holdup can be described by

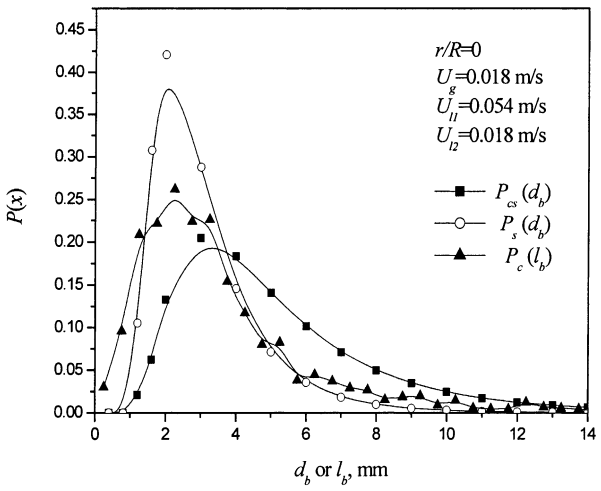

Fig. 5. Distributions of bubble size and chord length.

$$\varepsilon_g = \int_0^\infty m_b P_s(d_b) \frac{\pi\alpha}{6} \left(\frac{d_b}{\alpha}\right)^3 \mathrm{d}d_b$$
$$= m_b \frac{\pi}{6\alpha^2} \int_0^\infty P_s(d_b) d_b^3 \,\mathrm{d}d_b \quad (11)$$

where the shape factor α is consumed to be a constant. Similarly, the gas–liquid interfacial area can be described by

$$a = \int_0^\infty m_b P_s(d_b) \frac{\pi}{\alpha} d_b^2 \,\mathrm{d}d_b = m_b \frac{\pi}{\alpha} \int_0^\infty P_s(d_b) d_b^2 \,\mathrm{d}d_b \quad (12)$$

where

$$d_{va} = \int_0^\infty \frac{P_s(d_b) d_b^3}{P_s(d_b) d_b^2} \,\mathrm{d}d_b$$

is the bubble Sauter diameter. Substituting Eq. (12) into Eq. (11) leads to

$$a = \varepsilon_g \frac{6\alpha^2}{\pi} \left[\int_0^\infty P_s(d_b) d_b^3 \,\mathrm{d}d_b\right]^{-1} \frac{\pi}{\alpha} \int_0^\infty P_s(d_b) d_b^2 \,\mathrm{d}d_b$$
$$= \frac{6\alpha\varepsilon_g}{d_{va}} \quad (13)$$

Thus, the gas–liquid interfacial area can be determined with Eq. (13). Note that the value of the shape factor α is needed. Based on vast data in the literature Wellek et al. [15] proposed a correlation to predict the shape factor of droplets or bubbles

$$\alpha = \frac{1}{1 + 0.163\, Eo^{0.757}} \quad Mo \le 10^{-6}, Eo < 40 \quad (14)$$

where $Eo = g\rho_l d_e^2/\sigma$ is the Eötvös number and $Mo = g\mu_l^4/\rho_l\sigma^3$ the Morton number. Using this correlation and the bubble size distribution gives an approximate value 0.8 of the bubble average shape factor.

4. Result and discussion

4.1. Radial profile of the bubble size distribution

With the software for data acquisition and analysis, the bubble chord length and size distribution have been obtained, as shown in Fig. 5. The experimental results show that $P_s(d_b)$ can be described by lognormal function, in accordance with the results reported in CTPFBs without outer particle circulation [12,16].

The bubble Sauter diameter is not uniform in radial direction. In TPCFBs, the bubble Sauter diameter is smaller in the central region than that in the near wall region, different from CTPFBs without outer particle circulation [6]. This difference may be caused by the higher liquid velocity and outer particle circulation in TPCFBs. Considering that the gas holdup is higher in the central region [3], the profile of d_{va} in TPCFBs is favorable to enhance the gas–liquid interfacial area, which in turn, favorable to the gas–liquid mass transfer.

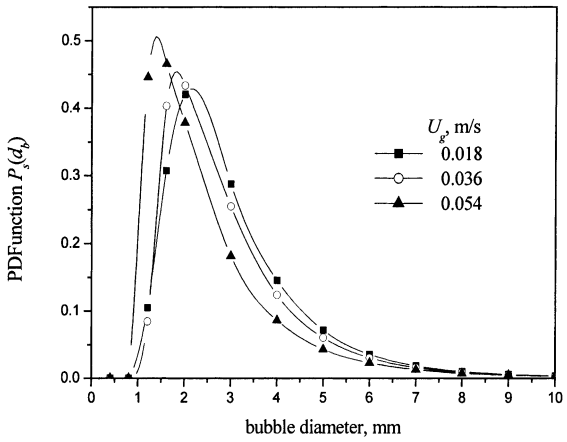

Fig. 6. Effect of superficial gas velocity on bubble size distribution at radial position $r/R = 0$.

4.2. Influence of operating conditions on bubble size distribution

4.2.1. Influence of superficial gas velocity

Figs. 6 and 7 illustrate the influence of U_g on $P_s(d_b)$. The bubble Sauter diameter decreases with increase of the superficial gas velocity within relatively lower U_g range, however, contrary results in CTPFBs are found in the literature [7,17]. The bubble size is influenced by the phase holdup, phase velocity, phase structure and the gas sparger structure. Whether this contrary is caused by the sparger structure or the special characteristics of TPCFBs needs further investigation. Although both the bubble Sauter diameter in the central region and near-wall region decreases when U_g increased, the variation in the near-wall region is more obviously, resulting in more uniform radial profile of d_{va} with increasing U_g as shown in Fig. 7.

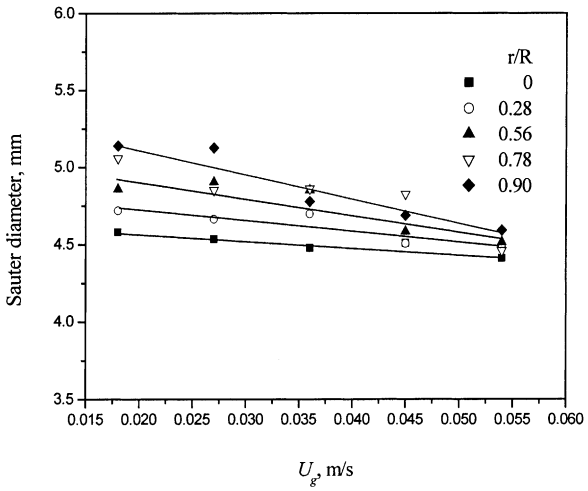

Fig. 7. Effect of superficial gas velocity on bubble Sauter diameter.

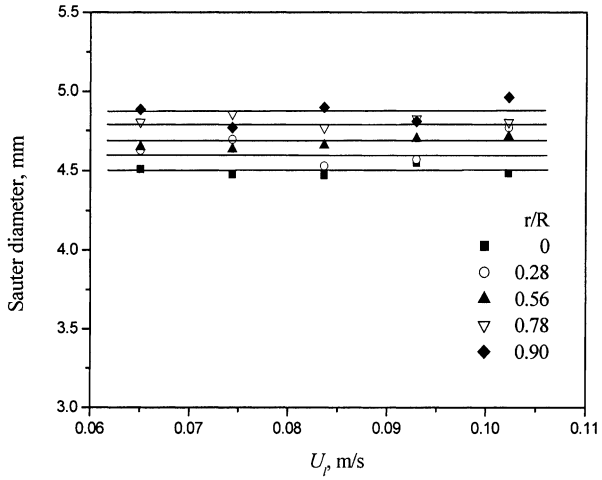

Fig. 8. Effect of superficial liquid velocity on bubble Sauter diameter.

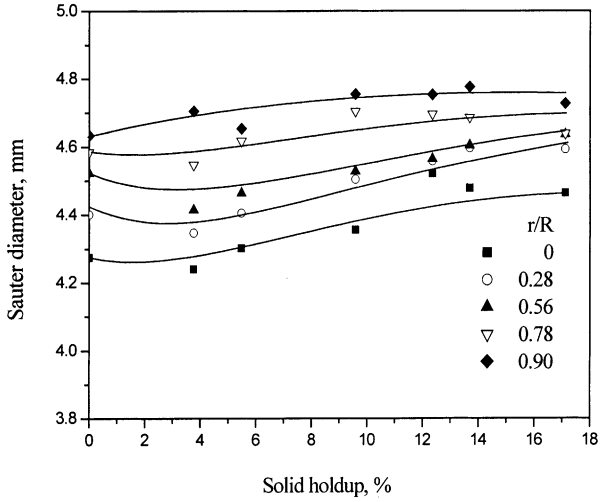

Fig. 9. Effect of solid holdup on bubble Sauter diameter.

4.2.2. Influence of superficial liquid velocity U_ℓ

The influence of U_ℓ on d_{av} in different radial position is shown in Fig. 8. The results show that U_ℓ has no significant influence on the bubble Sauter diameter in the circulating regime. Matsuura et al. [12] reported the bubble size decreases when U_ℓ increased. Lee et al. [15] found the similar result in the range of low liquid velocity, but nearly no variance of bubble size with U_ℓ was found when U_ℓ is higher than a certain value, in accordance with our experiment result in TPCFBs with higher liquid velocity.

4.2.3. Influence of particle circulation rate G_s

Particle circulation rate G_s can be controlled by changing the ratio of mainstream to secondary stream of the liquid. Generally speaking, solid holdup increases with particle circulating rate G_s [5]. The influence of solid holdup ε_s on d_{va} at different radial positions is shown in Fig. 9. The bubble Sauter diameter d_{va} decreases slightly with the increase of ε_s in the region of low ε_s, and it increases in the region of relatively higher ε_s. This may be caused by increase of apparent viscosity due to increased solid holdup.

4.3. Bubble rise velocity distribution

Due to the bubble size distribution and the turbulence of the gas and liquid phase, the bubble rise velocity u_b is non-uniform, as shown in Fig. 10. The distribution of

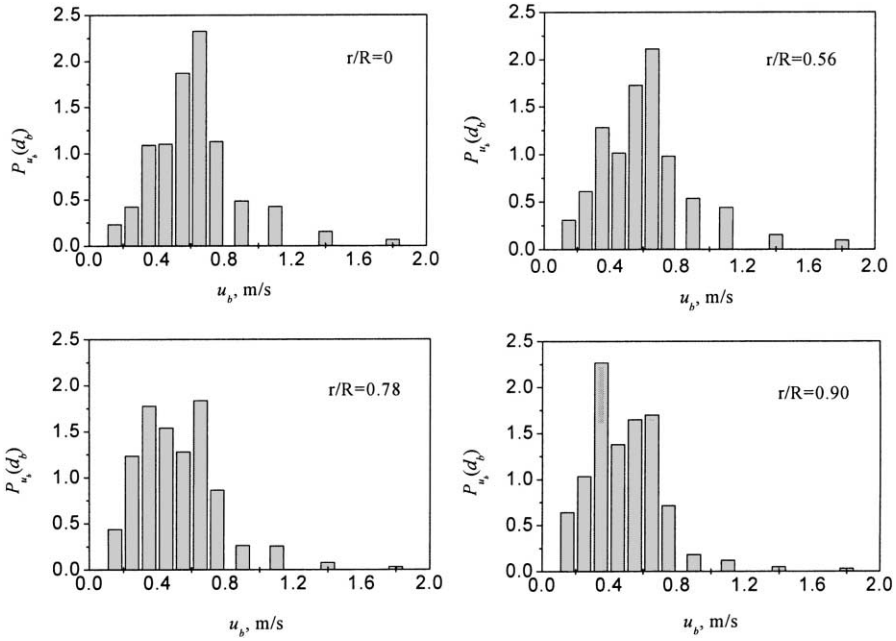

Fig. 10. Bubble rise velocity distribution at different radial position.

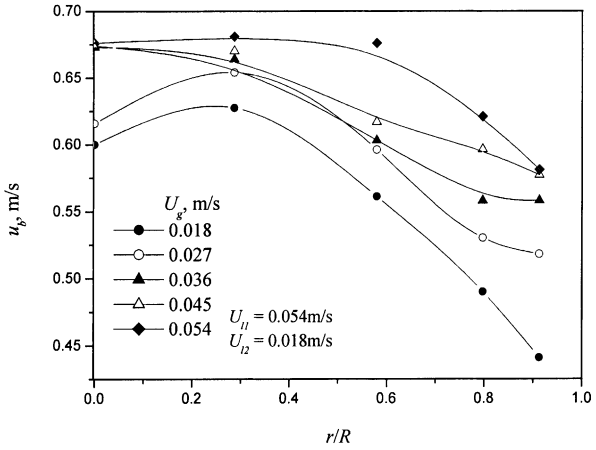

Fig. 11. Radial profile of bubble rise velocity.

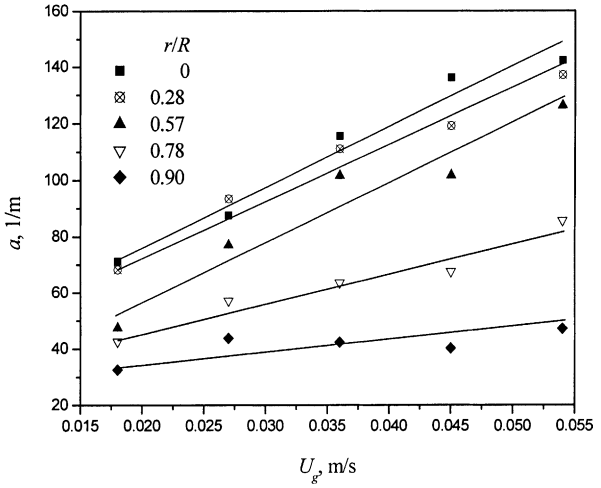

Fig. 12. Influence of U_g on a.

u_b in the central region has larger average value and smaller standard deviation than that in the near-wall region. The liquid velocity [5] and gas holdup [18] are higher in the central region, both favorable to increase the bubble rise velocity. The more scatter distribution of u_b in the near wall region may be explained that the distribution of u_b is mainly caused by the turbulence of liquid phase and gas phase. Large vortexes in dynamic equilibrium of formation and disintegration were observed in the near wall region, causing more violent turbulence and more scattered distribution of u_b.

The radial profile of the bubble rise velocity is shown in Fig. 11. In the case of low gas velocity ($U_g < 0.03$ m/s), the maximum bubble rise velocity occurs at the radial position $r/R \approx 0.2$, not at the center, probably due to the secondary spiral structure of bubble swarm. When the superficial gas velocity further increases, the radial profile of the bubble rise velocity becomes more uniform, especially in the region $r/R < 0.6$ when $U_g > 0.05$ m/s.

4.4. Influence of the operating conditions on the gas–liquid interfacial area

Based on the measured gas holdup and bubble size distribution, the gas–liquid interfacial area can be determined from Eq. (13), a shape factor of 0.8 is used based on Eq. (14). The influences of U_g, U_ℓ and G_s on the gas–liquid interfacial area are shown in Figs. 12–14, respectively. Both the outer particle circulation and relatively higher liquid velocity are favorable to the bubble breakup, so that the bubble Sauter diameter is relatively small and the variation of the bubble diameter is <15% under the experiment conditions. Thus, the interfacial area mainly depends on the gas holdup. When increasing the superficial gas velocity, the gas–liquid interfacial area increases more remarkably in the central region than in the near-wall region, as shown in Fig. 12. The liquid velocity has the contrary effect leading to more uniform radial profile of the gas–liquid interfacial area, as shown in

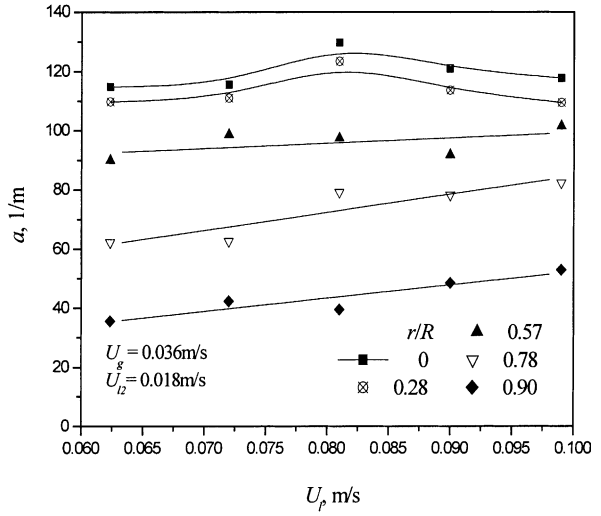

Fig. 13. Influence of U_l on a.

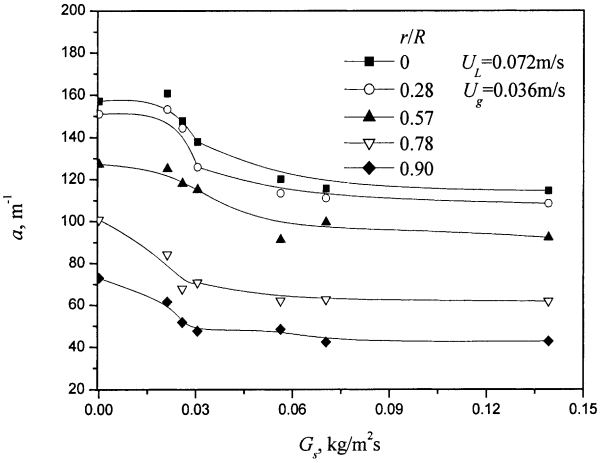

Fig. 14. Influence of G_s on a.

Fig. 13, which is favorable to enhance the efficiency of the reactor.

The influence of G_s on the gas–liquid interfacial area is shown in Fig. 14. A large particle circulation G_s causes remarkable decrease of the gas–liquid interfacial area due to the decrease of ε_g and increase of the bubble Sauter diameter.

5. Conclusions

The bubble size distribution, bubble rise velocity and local gas holdup have been measured in TPCFBs by an optic fiber probe system developed in this study, and the gas–liquid interfacial area has also been determined. Experimental study has resulted in the following conclusions:

- The bubble size distribution can be described by lognormal function. The bubble Sauter diameter, having the radial profile with smaller value in the central region, decreases with the gas velocity and increases with the particle circulation rate. The liquid velocity has no significant effect on the bubble size.
- The bubble rise velocity has larger average value and smaller standard deviation in the central region than in the near-wall region.
- The gas–liquid interfacial area obviously increases with the superficial gas velocity, slightly increases with the superficial liquid velocity, and decreases with G_s. The radial profile of the gas–liquid interfacial area becomes more uniform with increase of U_ℓ and more non-uniform with U_g.

Acknowledgements

Supported by the Chinese National Natural Science Foundation, No. 29876019.

References

[1] L.S. Fan, Gas–Liquid–Solid Fluidization Engineering, Butterworths, New York, 1989.
[2] W.G. Liang, Q.W. Wu, Y. Jin, H.T. Bai, Flow regimes of the three-phase circulating fluidized bed, AIChE J. 41 (2) (1995a) 267–271.
[3] W.G. Liang, Z.Q. Yu, Y. Jin, Hydrodynamics of a gas–liquid–solid three-phase circulating fluidized bed, Chem. Eng. J. 58 (1995b) 259–264.
[4] W.G. Yang, J.F. Wang, L.M. Zhou, Y. Jin, Gas–liquid mass transfer behavior in three-phase CFB reactors, Chem. Eng. Sci. 54 (1999a) 5523–5528.
[5] W.G. Yang, J.F. Wang, J. Zhou, Y. Jin, Liquid phase flow structure and backmixing characteristics of gas–liquid–solid three-phase circulating fluidized bed, Chem. Eng. Sci. 54 (1999b) 5293–5298.
[6] Z. Chen, C. Zheng, H. Hofmann, Local bubble behavior in three-phase fluidized beds, Can. J. Chem. Eng. 76 (1998) 315–318.
[7] W. Luewisutthichat, A. Tsutsumi, K.J. Yoshida, Bubble characteristics in multi-phase flow systems: bubble sizes and size distributions, J. Chem. Eng. Jpn. 30 (1997) 461–466.
[8] W. Liu, N.N. Clark, A.I. Karamavruc, Relationship between bubble size distributions and chord-length distribution in heterogeneously bubbling systems, Chem. Eng. Sci. 53 (1998) 1267–1276.
[9] S. Saberi, K. Shakourzadeh, D. Bastoul, J. Militzer, Bubble size and velocity measurement in gas–liquid systems: application of fiber optic technique to pilot plant scale, Can. J. Chem. Eng. 70 (1995) 253–257.
[10] R.P. Roy, V. Velidandla, S.P. Kalra, P. Peturaud, Local measurements in the two-phase region of turbulent subcooled boiling flow, Trans. ASME 116 (8) (1994) 660–669.
[11] C.D. Serdula, M.R. Loewen, Experiments investigating the use of fiber-optic probes for measuring bubble-size, IEEE J. Ocean Eng. 23 (4) (1998) 385–399.
[12] A. Matsuura, L.S. Fan, Distribution of bubble properties in a gas–liquid–solid fluidized bed, AIChE J. 30 (6) (1984) 894–903.
[13] C. Alain, Optical probes for local void fraction measurements: characterization of performance, Rev. Sci. Instrum. 62 (2) (1990) 874–886.
[14] K. Tsuchiya, A. Furumoto, L.S. Fan, J.P. Zhang, Suspension viscosity and bubble rise velocity in liquid–solid fluidized beds, Chem. Eng. Sci. 52 (18) (1997) 3053–3066.
[15] R.M. Wellek, A.K. Agrawal, A.H.P. Skelland, Shape of liquid drops moving in liquid media, AIChE J. 12 (1966) 854–862.
[16] J.C. Lee, H. Worthington, Chem. Engs. Symposium Series, No. 38, Multi-Phase Flow Systems, Inst. Chem. Engs., London, 1974.
[17] M. Fukuma, K. Muroyama, A. Yasunishi, Properties of bubble swarm in a slurry bubble column, J. Chem. Eng. Jpn. 20 (1) (1987) 28–33.
[18] T.F. Wang, J.F. Wang, W.G. Yang, Y. Jin, Experimental study on gas-holdup and gas–liquid interfacial area in TPCFBs, Chem. Eng. Comm., in press.
[19] A. Mntsuura, L.S. Fan, Distribution of bubble properties in a gas-liquid-solid fluidized bed, AIChE J. 30 (6) (1984) 894–903.